Resolution-Enhanced Ptychographic Modulation Imaging via Divergent Illumination

Jun Lan, Cheng Xu, Hui Pang, Song Hu, and Yong Yang

***Abstract*—By inserting a modulator in the imaging system and scanning in different positions, ptychographic modulation imaging can achieve higher quality reconstruction for smooth or weakly scattered objects compared to conventional ptychography imaging. However, its imaging resolution is still limited by the pixel size of the detector. In this paper, divergent illumination is introduced to enhance imaging resolution. Compared with the original planar illumination scheme, our proposed method can achieve two-fold resolution improvement with only the use of thirty diffraction patterns for ten iterations. The quantitative phase imaging capability of the proposed method is also demonstrated by testing the binary phase sample. In the reconstruction, the divergent illumination geometry is converted to planar illumination model. The equivalent sampling intervals and diffraction distances of the modulator, object, and detector planes are analyzed in detail. In addition, a new high-accuracy distance calibration method for point light sources is proposed and verified in experiments.**

***Index Terms*—Coded coherent diffraction imaging, phase retrieval, divergent illumination.**

I. Introduction

PHASE conveys crucial characteristic information of the object. Nevertheless, current detectors are only able to record amplitude information since the frequency of light is much higher than the detector's response frequency, and thus the phase information is missed. Coherent diffraction imaging (CDI) is an excellent technique used to reconstruct complex objects from recorded diffraction intensity patterns by utilizing the iterative phase retrieval algorithm. [1], [2], [3]. At present, CDI has been successfully applied to materials science, crystallography, biological sample observation, and other fields with its compact and highly robust experimental setup [4], [5], [6]. Certainly, phase retrieval algorithms using multiple diffraction patterns as constraints enable higher accuracy in reconstructing complex objects than the pioneering work using only a single diffracted light intensity [7]. In general, there are two most common configurations. One strategy is to scan the detector axially along the optical axis and record the diffraction patterns over different locations. Through iterative diffraction calculations between the object plane and a series of measurement planes, the complex wavefront of the object can be retrieved without prior knowledge [8], [9], [10], [11], [12]. Ptychography imaging with spatially confined illumination is another strategy that captures hundreds of diffraction intensities by laterally moving the object with a localized probe beam at several grid positions [13], [14]. Since the neighboring illumination regions overlap with each other, abundant redundant information is generated and effectively solves the ambiguity problem in the phase retrieval process. Nevertheless, these methods will be hampered for smooth or weakly scattered objects because the variation of the recorded diffraction patterns is not insufficient [15]. To solve this problem, ptychographic modulation imaging technology is proposed. Specifically, a thin unknown modulator is inserted between the object and the detector, by laterally shifting the modulator, a sequence of strongly varying modulated intensity is recorded for the object reconstruction [16]. Afterward, numerous studies were conducted about the optimization of experimental setup layouts for simplified operation [17], [18], [19], [20]. However, according to the Nyquist sampling theorem, the inherent problem that the reconstruction resolution of the object is limited by the pixel size of the detector used in the experiment still exists in the modulated imaging system [21], [22].

Considering the intrinsic scalability of the spherical wave illumination scheme [23], [24], [25]. In this paper, we introduce divergent illumination into the ptychographic modulation imaging to break through the limitation of the pixel size of the detector used in the experiment on the image resolution. In the reconstruction process, the divergent illumination is converted to equivalent planar illumination scheme based on the scaling theorem. The equivalent sampling intervals and diffraction distances of the modulator, object, and detector planes are analyzed in detail. In addition, a new distance calibration method for point light sources is proposed.

Manuscript received 18 December 2023; revised 27 February 2024; accepted 3 March 2024. Date of publication 8 March 2024; date of current version 21 March 2024. This work was supported in part by the West Light Foundation of the Chinese Academy of Sciences under Grant xbzg-zdsys-202315 and in part by Sichuan Regional Innovation Cooperation Project under Grant 2023YFQ0108. *(Corresponding author: Yong Yang).*

Jun Lan, Hui Pang, Song Hu, and Yong Yang are with the National Key Laboratory of Optical Field Manipulation Science and Technology, Chinese Academy of Sciences, Chengdu 610209, China, also with the State Key Laboratory of Optical Technologies on Nano-Fabrication and Micro-Engineering, Institute of Optics and Electronics, Chinese Academy of Sciences, Chengdu 610209, China, also with the Institute of Optics and Electronics, Chinese Academy of Science, Chengdu 610209, China, and also with the University of Chinese Academy of Sciences, Beijing 100049, China (e-mail: lanjun19@mails.ucas.ac.cn; wuli041@126.com; husong@ioe.ac.cn; yoyo955@163.com).

Cheng Xu is with the Institute of Optics and Electronics, Chinese Academy of Science, Chengdu 610209, China, and also with the School of Physics, University of Electronic Science and Technology of China, Chengdu 610054, China (e-mail: xucheng_666@126.com).

Digital Object Identifier 10.1109/JPHOT.2024.3373806

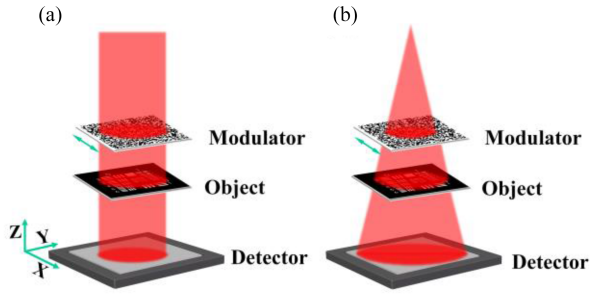

Fig. 1. Comparison between the (a) planar illumination and (b) the divergent illumination.

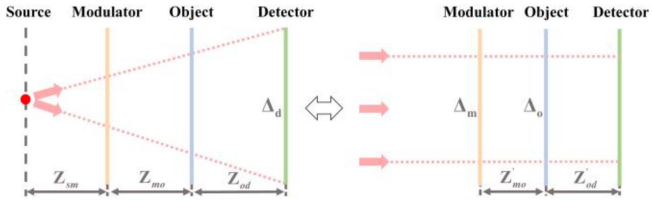

Fig. 2. Conversion of the divergent illumination model to the equivalent planar illumination model.

II. Methodology

A. System Setup

The ptychographic modulation imaging experiments with two different illumination schemes have been conducted in this paper. Specifically, Fig. 1(a) shows the schematic diagram of the planar illumination experimental configuration. A collimated laser beam is modulated by a random binary amplitude mask and yields a speckle field on the surface of the object. Afterward, the complex exit wavefront from the object propagates for a fixed distance and is recorded by the detector. By moving the modulator laterally along the x-axis, variable speckle fields can be generated on the object's surface. Each time the mask moves, the detector records a corresponding diffraction intensity which carries the information about the object. Finally, combined with the extended ptychographic iterative engine (ePIE) algorithm [26], the complex amplitude of the object and speckle field can be reconstructed simultaneously. It's worth mentioning that it is also feasible for the modulator to move both in the x-axis and y-axis, and the reconstruction model established in this paper is still applicable to this movement mode when the y-axis offset is considered. The schematic diagram for the proposed method of divergent illumination is shown in Fig. 1(b). Compared to Fig. 1(a), the main difference lies in that the collimated plane wave illumination is replaced by the divergent illumination from a point light source.

B. Scaling Principle

The divergent illumination can be converted to equivalent planar illumination model based on the Fresnel propagation theorem. The schematic diagram of the conversion of the sampling interval and diffraction distance is shown in Fig. 2. In the divergent illumination scheme, the exiting wave of the object plane will be magnified in the detector plane, which is equivalent to de-magnify the physical pixel size of the detector and can be described as

$$\Delta_o = \frac{\Delta_d}{M_{od}}, \tag{1}$$

where Δ_d and Δ_o represent the actual physical pixel size of the detector and the equivalent sampling interval used in the object reconstruction process, respectively, M_{od} is the scaling factor of the object plane in the detector plane and can be calculated as

$$M_{od} = \frac{Z_{sm} + Z_{mo} + Z_{od}}{Z_{sm} + Z_{mo}}, \tag{2}$$

Where Z_{sm} is the distance between the source and modulator, $Z_{mo}$is the distance between the modulator and object, and the Z_{od} is the distance between the object and detector.

Furthermore, the equivalent distance between the object plane and the detector plane is shortened to

$$Z'_{od} = \frac{Z_{od}}{M_{od}}. \tag{3}$$

Particularly, in this work, the object is placed between the modulator and the detector. Hence, by using the above parameters combined with the ePIE algorithm, the complex amplitude distribution of the object and speckle field at the object plane can be recovered simultaneously. Then, by backward propagating the speckle field from the object plane to the modulator plane, the complex amplitude distribution of the modulator can be retrieved. It is worth noting that the propagation of divergent light between the modulator plane and the object plane can also lead to scaling issues, and the corresponding equivalent pixel size used in the modulator reconstruction process can be written as

$$\Delta_m = \frac{\Delta_o}{M_{mo}}, \tag{4}$$

where M_{mo} is the scaling factor of the modulator plane in the object plane, which is determined by

$$M_{mo} = \frac{Z_{sm} + Z_{mo}}{Z_{sm}}, \tag{5}$$

Similarly, the effective backpropagation distance from the object to the modulator can be described as

$$Z'_{mo} = \frac{Z_{mo}}{M_{mo}}. \tag{6}$$

C. Reconstruction Algorithm

It is emphasized that the whole reconstruction process is based on the equivalent planar illumination model. Suppose the speckle field formed by the modulator in the object surface is$S(x1, y1)$, the complex amplitude distribution of the object is $O(x1, y1)$. At the beginning, both $S(x1, y1)$ and $O(x1, y1)$are initialized to all-one matrix. When the modulator moves to the *n*th position along the *x*-axis, the corresponding speckle field on the object plane is expressed as

$$S_n(x1, y1) = S(x1 - d_n, y1), \tag{7}$$

where $n = 1,2,\ldots,$ N. The position $(x1 - d_n, y1)$ can be determined through cross-correlation operation. The complex wavefront that exits from the object plane can be denoted as

$$T_n(x1, y1) = O(x1, y1) \cdot S_n(x1, y1). \tag{8}$$

Subsequently, the exiting wavefront is free-space propagation from the object to the detector, which can be written as

$$\begin{aligned} U_n(x2, y2) &= A\left\{T_n(x1, y1), \Delta_o, Z'_{od}\right\}, \\ &= F^{-1}\Bigg\{F\left[T_n(x1, y1)\right] \exp \\ &\quad \left[\left(i\frac{2\pi}{\lambda}Z'_{od}\right)\sqrt{1-\lambda^2 f_{xo}^2 - \lambda^2 f_{yo}^2}\right]\Bigg\}. \end{aligned} \tag{9}$$

where $A\{\}$ denotes the angular spectrum method for calculating the light propagation. F and F^{-1} represent the Fourier transform and the inverse Fourier transform, respectively.

After that, the modulus of $U_n(x2, y2)$is replaced by the square root of the recorded intensity. The new estimated wavefront is given by

$$U'_n(x2, y2) = \sqrt{I_n(x2, y2)} \exp\left[i\psi_n(x2, y2)\right]. \tag{10}$$

where $I_n(x2, y2)$ is the diffraction pattern recorded by the detector which corresponds to the nth shift of the modulator, $\psi_n(x2, y2)$ denote the phase of $U_n(x2, y2)$. The modified wavefront $U'_n(x2, y2)$ then propagates back to the object plane, and the new wavefront $T'_n(x1, y1)$ can be calculated as

$$\begin{aligned} T'_n(x1, y1) &= A\left\{U'_n(x2, y2), \Delta_o, -Z'_{od}\right\}, \\ &= F^{-1}\Bigg\{F\left[U'_n(x2, y2)\right] \exp \\ &\quad \left[\left(-i\frac{2\pi}{\lambda}Z'_{od}\right)\sqrt{1-\lambda^2 f_{xo}^2 - \lambda^2 f_{yo}^2}\right]\Bigg\}. \end{aligned} \tag{11}$$

By using the ePIE algorithm, both the complex object and speckle field at the object plane can be updated simultaneously as follows

$$\begin{aligned} O^{update}(x1, y1) &= O(x1, y1) + \frac{S_n^*(x1, y1)}{|S_n(x1, y1)|^2_{\max}} \\ &\quad \cdot \left[T_n{}'(x1, y1) - T_n(x1, y1)\right], \\ S_n^{update}(x1, y1) &= S_n(x1, y1) + \frac{O^*(x1, y1)}{|O(x1, y1)|^2_{\max}} \\ &\quad \cdot \left[T_n{}'(x1, y1) - T_n(x1, y1)\right]. \end{aligned} \tag{12}$$

Then, the overall speckle field is revised by

$$S(x1 - d_n, y1) = S_n^{update}(x1, y1). \tag{13}$$

After the recorded N diffraction patterns are processed as above, it means a single iteration is completed. Further, dozens of iterations are enough to reconstruct the complex object.

The above iterations have completed the recovery of complex object and speckle field in the object plane. Thereafter, the complex amplitude distribution of the modulator can be obtained by backward propagation of the speckle field as follows

$$\begin{aligned} M(x0, y0) &= A\left\{S(x1, y1), \Delta_m, -Z'_{mo}\right\}, \\ &= F^{-1}\Bigg\{F\left[S(x1, y1)\right] \exp \\ &\quad \left[\left(-i\frac{2\pi}{\lambda}Z'_{mo}\right)\sqrt{1-\lambda^2 f_{xm}^2 - \lambda^2 f_{ym}^2}\right]\Bigg\}. \end{aligned} \tag{14}$$

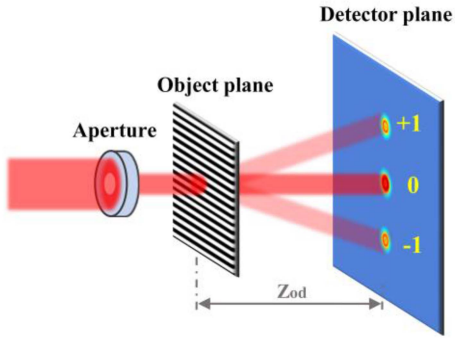

Fig. 3. Schematic diagram of the grating measuring distance.

Generally, the advantage of divergent illumination configuration is that it has the inherent characteristics of shortening the effective distance between the object and the detector and reducing the effective sampling intervals during reconstruction. In other words, it can enhance the imaging resolution of the system under the same configuration parameters. Actually, in our scheme, the recovery of the modulator can be omitted, thus not only reducing computation time but also eliminating the need for measuring the distance between the modulator and the object. Nevertheless, for some schemes where the object is placed upstream of the modulator, that means the position relationship between the object and the modulator is opposite to our experimental setup. For this scheme, the complex object distribution cannot be directly retrieved by using the ePIE algorithm and the backward propagation step becomes necessary.

D. Distance Determination

In the phase retrieval technique, the measurement accuracy of the object-to-detector distance is one of the most critical factors affecting the reconstruction quality. In this study, a transmission grating is used to measure this distance, and the corresponding calculation principle is shown in Fig. 3. Specifically, a transmission grating with the known period is placed in the plane of the object, and its corresponding diffraction intensity is recorded by the detector. By computing the spacing between the zero-order and first-order diffraction spots, the distance Z_{od} can be easily obtained by using the grating equation [27].

$$Z_{od} = \frac{L}{\tan(\arcsin(\lambda/P))}, \tag{15}$$

Where L is half of the distance between the $+1$th and the -1th light spot, λ is the wavelength of the laser source, and P is the known grating period.

In addition, the determination of the distance between the point light source and the object is also a critical step in the divergent illumination experiment. Here, we propose a new and more implementable approach than the previous study [28], and

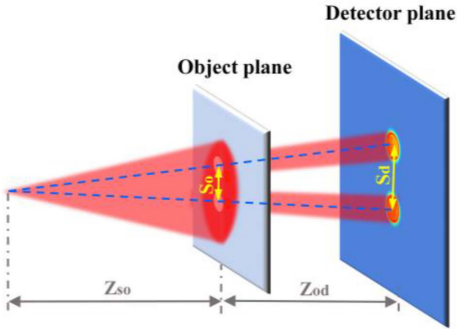

Fig. 4. Determination of the distance between the point source and object.

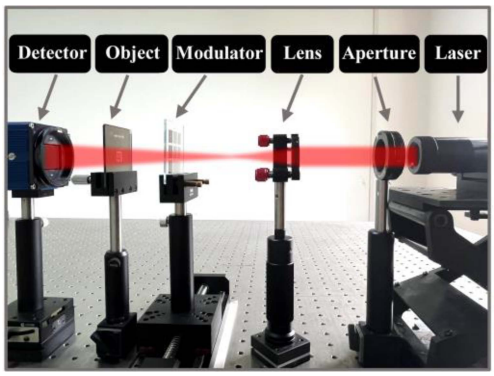

Fig. 5. Experimental setup of the proposed ptychographic modulation imaging.

the corresponding schematic is illustrated in Fig. 4. A specific binary mask with two millimeter-sized holes separated with a distance S_o is placed on the object plane. Then, the spacing of the diffraction pattern S_d generated by these holes is determined through cross-correlation [16]. Given the distance from the object to the detector has been obtained by using the transmission grating, the distance from the point light source to the object plane can be solved according to the similar triangle relationship.

$$\frac{S_o}{S_d} = \frac{Z_{so}}{Z_{so} + Z_{od}}. \tag{16}$$

It should be noted that these two approaches are not limited to measuring the distance between the above-mentioned planes. Moreover, they hold significant application value in distance calibration of the phase recovery technology domain.

III. Experimental Results

The experiment setup shown in Fig. 5 is established to verify the effectiveness of our proposed method. A collimated laser beam with a wavelength of 650 nm is utilized. Besides, the binary amplitude mask is adopted as a modulator, which is fabricated on a chrome-faced glass substrate by using lithography and installed on a motorized translation stage. A commercial CCD camera with a pixel count of 4898×3248 and pixel size of 7.4 μm × 7.4 μm is used to record the diffraction pattern. In the distance determination operation, a grating with a periodicity of 10 μm is employed, and the calculated distance is $Z_{od} = 70.36$ mm. Then a specialized mask is utilized, which features two small holes

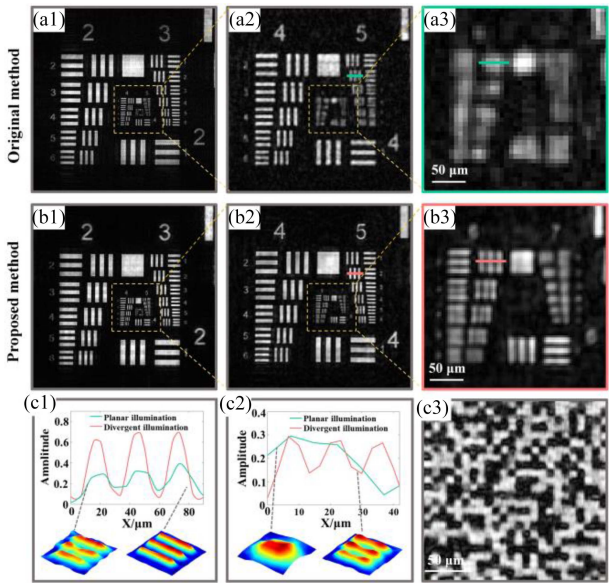

Fig. 6. Comparing the reconstruction results of the USAF 1951 resolution target. (a1–a3) the reconstructed results by planar illumination, (b1–b3) the reconstructed results by divergent illumination. The profile line and topography of group 5, element 2 (c1), and group 6, element 2, and (c2) by using two different methods. (c3) The reconstructed result of mask by divergent illumination.

with a diameter of 1 mm, positioned at a separation distance of 2 mm, and the determined distance is $Z_{so} = 56.17$ mm. What's more, when applying the planar illumination configuration, the converging lens should be removed from the optical system.

The 1951 USAF resolution target is initially used as an amplitude test sample. The modulator moves 30 times along the x-direction, and the detector captures the corresponding diffraction patterns. The central 1280 × 1280 pixels of these patterns serve as amplitude constraints and are fed into the reconstruction algorithm. The comparison of the reconstruction results between two different schemes is illustrated in Fig. 6. Fig. 6(a1)–(a3) represents the results obtained using the original planar illumination. It is shown that group 5, element 2 can be resolved and the corresponding resolution is 13.92 μm (36 lp/mm). It can be further seen that there is a mosaic-like phenomenon in Fig. 6(a3), which is actually caused by the limitation of the detector pixel size on the imaging resolution. The results of the proposed divergent illumination are shown in Fig. 6(b1)–(b3) and (c3). It is evident that the lines in group 6, element 2 are distinguishable, achieving a resolution of 6.96 μm (71.8 lp/mm). The profile line and topography of group 5, element 2, recovered by two methods, are presented in Fig. 6(c1). In the same way, Fig. 6(c2) displays the profile line and topography of group 6, element 2. It is not difficult to find that the proposed method can achieve enhanced contrast and high precision in reconstructing amplitude object, and it obtains twice the resolution of the traditional method. What's more, our method successfully overcomes the constraint imposed by the detector's pixel size (7.4 μm) on imaging resolution.

The quantitative phase imaging capability of our proposed method is also demonstrated and the experimental parameters are same as the previous experiment. In this study, a phase sample with the lotus pattern and fabrication on a silica substrate

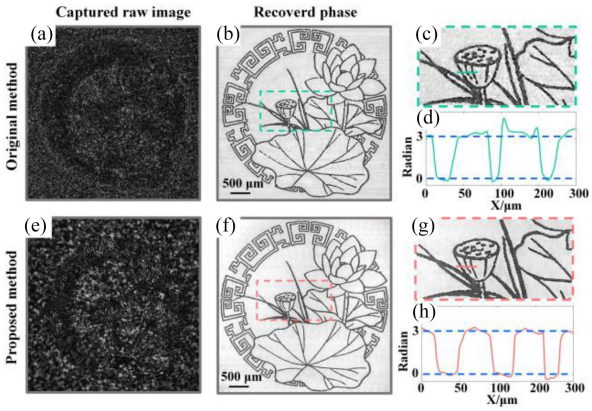

Fig. 7. Comparing the reconstruction results of the phase object. (a) The captured raw image, (b) the reconstruction result, (c) the corresponding partial enlargement with the original method, (e) the captured raw image, (f) the reconstruction result, and (g) the corresponding partial enlargement with the proposed method. The comparison of the phase profile lines is plotted in (d) and (h).

through lithography is adopted. Specifically, the pattern profile depth measured by the step profiler is about 725 nm, so the true phase delay is equal to 3.2 rad. Fig. 7(a)–(d) are the retrieved results using planar illumination. Specifically, Fig. 7(a) shows the captured raw image and Fig. 7(b) is the retrieved phase distribution of the object. Moreover, Fig. 7(c) is the magnification of the green dashed box area in Fig. 7(b), and the phase profile of the green line is shown in Fig. 7(d). Furthermore, Fig. 7(e)–(h) represents the corresponding results by using divergent illumination. Both methods successfully recover the outline of the phase object, but our proposed method yields more distinct and refined results. Additionally, our configuration demonstrates a closer alignment with the actual depth of the phase target, as indicated by the blue lines in Fig. 7(d) and (h). This also highlights the superior quantitative phase imaging ability of our method.

IV. Summary

In conclusion, this study introduces divergent illumination into the ptychographic modulation imaging and effectively solves the limitation of detector pixel size on imaging resolution. Experimental results show that compared with the original planar illumination scheme, the proposed method can reconstruct both amplitude and phase objects with higher precision and successfully breaks through the resolution limitation of detector pixel size. We also comprehensively analyzed the scaling principle of the multi-plane model and proposed a novel distance calibration method for divergent illumination configuration. The results of the proposed method can be further improved by optimizing the experimental parameter settings or by using detectors with smaller pixels. The suggested method possesses the potential to become a simple means to achieve pixel super-resolution in phase retrieval technique, holding great promise for applications in coherent diffraction imaging.

References

[1] J. R. Fienup, "Reconstruction of an object from the modulus of its Fourier transform," *Opt. Lett.*, vol. 3, no. 1, pp. 27–29, 1978.

[2] J. R. Fienup, "Phase retrieval algorithms: A comparison," *Appl. Opt.*, vol. 21, no. 15, pp. 2758–2769, 1982.

[3] R. A. Dilanian et al., "Coherent diffractive imaging: A new statistically regularized amplitude constraint," *New J. Phys.*, vol. 12, no. 9, 2010, Art, no. 093042.

[4] S. Takazawa, J. Kang, M. Abe, H. Uematsu, N. Ishiguro, and Y. Takahashi, "Demonstration of single-frame coherent X-ray diffraction imaging using triangular aperture: Towards dynamic nanoimaging of extended objects," *Opt. Exp.*, vol. 29, no. 10, pp. 14394–14402, 2021.

[5] P. F. Almoro, G. Pedrini, P. N. Gundu, W. Osten, and S. G. Hanson, "Phase microscopy of technical and biological samples through random phase modulation with a diffuser," *Opt. Lett.*, vol. 35, no. 7, pp. 1028–1030, 2010.

[6] A. Maiden, D. Johnson, and P. Li, "Further improvements to the ptychographical iterative engine," *Optica*, vol. 4, no. 7, pp. 736–745, 2017.

[7] R. W. Gerchberg and W. O. Saxton, "A practical algorithm for the determination of phase from image and diffraction plane pictures," *Optik.*, vol. 35, no. 2, pp. 237–250, 1972.

[8] G. Pedrini, W. Osten, and Y. Zhang, "Wave-front reconstruction from a sequence of interferograms recorded at different planes," *Opt. Lett.*, vol. 30, no. 8, pp. 833–835, 2005.

[9] C. R. L. Buco and P. F. Almoro, "Enhanced multiple-plane phase retrieval using adaptive support," *Opt. Lett.*, vol. 44, no. 24, pp. 6045–6048, 2019.

[10] C. Xu et al., "Enhancing multi-distance phase retrieval via unequal interval measurements," *Photon..*, vol. 8, no. 2, 2021, Art. no. 48.

[11] J. F. Binamira and P. F. Almoro, "Accelerated single-beam multiple-intensity reconstruction using unordered propagations," *Opt. Lett.*, vol. 44, no, no. 12, pp. 3130–3133, 2019.

[12] J. M. Rodenburg and H. M. L. Faulkner, "A phase retrieval algorithm for shifting illumination," *Appl. Phys. Lett.*, vol. 85, no. 20, pp. 4795–4797, 2004.

[13] F. Zhang et al., "Translation position determination in ptychographic coherent diffraction imaging," *Opt. Exp.*, vol. 21, no. 11, 2013, Art. no. 13592.

[14] H. M. L. Faulkner and J. M. Rodenburg, "Movable aperture lensless transmission microscopy: A novel phase retrieval algorithm," *Phys. Rev. Lett.*, vol. 93, no. 2, 2004, Art. no. 023903.

[15] T. J. T. Abregana and P. F. Almoro, "Phase retrieval by amplitude modulation using digital micromirror device," *Opt. Laser Eng.*, vol. 150, 2022, Art. no. 106851.

[16] S. Jiang et al., "Wide-field, high resolution lensless on-chip microscopy via near-field blind ptychographic modulation," *Lab Chip.*, vol. 20, no. 6, pp. 1058–1065, 2020.

[17] H. Zhang, Z. Bian, S. Jiang, J. Liu, P. Song, and G. Zheng, "Field-portable quantitative lensless microscopy based on translated speckle illumination and sub-sampled ptychographic phase retrieval," *Opt. Lett.*, vol. 44, no. 8, pp. 1976–1979, 2019.

[18] X. Wen et al., "Ptychography imaging by 1-D scanning with a diffuser," *Opt. Exp.*, vol. 28, no. 15, pp. 22658–22668, 2020.

[19] C. Lu et al., "Mask-modulated lensless imaging via translated structured illumination," *Opt. Exp.*, vol. 29, no. 8, pp. 12491–12501, 2021.

[20] A. Hassan, S. Khan, K. Rasul, and A. Hussain, "Lensless on-chip LED array microscope using amplitude and phase masks," *J. Opt. Soc. Amer. B*, vol. 37, no. 12, pp. 3652–3659, 2020.

[21] C. E. Shannon, "Communication in the presence of noise," *Proc. IRE.*, vol. 37, no. 1, pp. 10–21, Jan. 1949.

[22] M. Li, T. Qin, Z. J. Gao, and L. H. Bian, "Illumination schemes for coded coherent diffraction imaging: A comprehensive comparison," *Opt. Laser Technol.*, vol. 168, 2024, Art, no. 109861.

[23] D. M. Paganin, "Coherent X-ray optics," Ph.D. dissertation, New York, NY, USA: Oxford Univ. Press, 2006.

[24] X. L. He, S. P. Veetil, Z. L. Jiang, Y. Kong, S. Y. Wang, and C. Liu, "High-speed coherent diffraction imaging by varying curvature of illumination with a focus tunable lens," *Opt. Exp.*, vol. 28, no. 17, pp. 25655–25663, 2020.

[25] D. Claus, G. Pedrini, and W. Osten, "Iterative phase retrieval based on variable wavefront curvature," *Appl. Opt.*, vol. 56, no. 13, pp. F134–F137, 2017.

[26] A. M. Maiden and J. M. Rodenburg, "An improved ptychographical phase retrieval algorithm for diffractive imaging," *Ultramicroscopy*, vol. 109, no. 10, pp. 1256–1262, 2009.

[27] C. Xu, H. Pang, A. Cao, and Q. H. Deng, "Enhanced multiple-plane phase retrieval using a transmission grating," *Opt. Laser Eng.*, vol. 149, 2022, Art. no. 106810.

[28] Y. Wagatsuma, T. Shimobaba, Y. Yamamoto, I. Hoshi, T. Kakue, and T. Ito, "Phase retrieval using axial diffraction patterns and a ptychographic iterative engine," *Appl. Opt.*, vol. 59, no. 2, pp. 354–362, 2020.